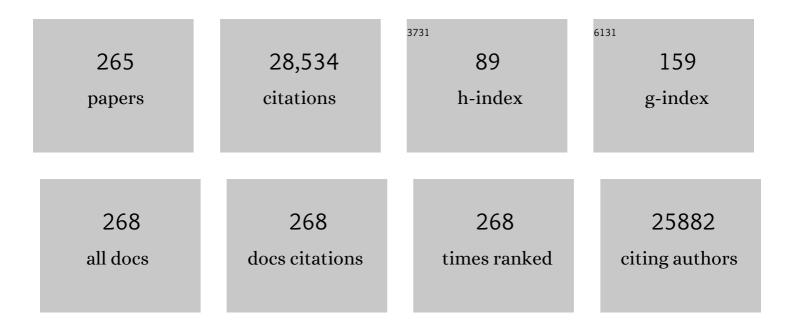
List of Publications by Year in descending order

Source: https://exaly.com/author-pdf/5172210/publications.pdf Version: 2024-02-01



#	Article	IF	CITATIONS
1	Ordered Mesoporous Black TiO ₂ as Highly Efficient Hydrogen Evolution Photocatalyst. Journal of the American Chemical Society, 2014, 136, 9280-9283.	13.7	878
2	Phosphorusâ€Ðoped Carbon Nitride Tubes with a Layered Microâ€nanostructure for Enhanced Visibleâ€Light Photocatalytic Hydrogen Evolution. Angewandte Chemie - International Edition, 2016, 55, 1830-1834.	13.8	869
3	From coconut shell to porous graphene-like nanosheets for high-power supercapacitors. Journal of Materials Chemistry A, 2013, 1, 6462.	10.3	794
4	Nitrogen-doped graphene with high nitrogen level via a one-step hydrothermal reaction of graphene oxide with urea for superior capacitive energy storage. RSC Advances, 2012, 2, 4498.	3.6	696
5	Molecule Self-Assembly Synthesis of Porous Few-Layer Carbon Nitride for Highly Efficient Photoredox Catalysis. Journal of the American Chemical Society, 2019, 141, 2508-2515.	13.7	685
6	Surface tuning for oxide-based nanomaterials as efficient photocatalysts. Chemical Society Reviews, 2013, 42, 9509.	38.1	564
7	Effects of Simultaneously Doped and Deposited Ag on the Photocatalytic Activity and Surface States of TiO2. Journal of Physical Chemistry B, 2005, 109, 2805-2809.	2.6	523
8	Integrating the active OER and HER components as the heterostructures for the efficient overall water splitting. Nano Energy, 2018, 44, 353-363.	16.0	516
9	Phosphorusâ€Modified Tungsten Nitride/Reduced Graphene Oxide as a Highâ€Performance, Nonâ€Nobleâ€Metal Electrocatalyst for the Hydrogen Evolution Reaction. Angewandte Chemie - International Edition, 2015, 54, 6325-6329.	13.8	515
10	Anionâ€Modulated HER and OER Activities of 3D Ni–Vâ€Based Interstitial Compound Heterojunctions for Highâ€Efficiency and Stable Overall Water Splitting. Advanced Materials, 2019, 31, e1901174.	21.0	479
11	Holey Reduced Graphene Oxide Coupled with an Mo ₂ N–Mo ₂ C Heterojunction for Efficient Hydrogen Evolution. Advanced Materials, 2018, 30, 1704156.	21.0	459
12	Co Nanoislands Rooted on Co–N–C Nanosheets as Efficient Oxygen Electrocatalyst for Zn–Air Batteries. Advanced Materials, 2019, 31, e1901666.	21.0	455
13	Wellâ€Ordered Largeâ€Pore Mesoporous Anatase TiO ₂ with Remarkably High Thermal Stability and Improved Crystallinity: Preparation, Characterization, and Photocatalytic Performance. Advanced Functional Materials, 2011, 21, 1922-1930.	14.9	431
14	Facile solvothermal synthesis of hierarchical flower-like Bi ₂ MoO ₆ hollow spheres as high performance visible-light driven photocatalysts. Journal of Materials Chemistry, 2011, 21, 887-892.	6.7	427
15	Synthesis of Particulate Hierarchical Tandem Heterojunctions toward Optimized Photocatalytic Hydrogen Production. Advanced Materials, 2018, 30, e1804282.	21.0	411
16	Interfacial Engineering of MoO ₂ â€FeP Heterojunction for Highly Efficient Hydrogen Evolution Coupled with Biomass Electrooxidation. Advanced Materials, 2020, 32, e2000455.	21.0	401
17	Effects of Surface Oxygen Vacancies on Photophysical and Photochemical Processes of Zn-Doped TiO2Nanoparticles and Their Relationships. Journal of Physical Chemistry B, 2006, 110, 17860-17865.	2.6	397
18	Nitrogenâ€Doped Porous Graphitic Carbon as an Excellent Electrode Material for Advanced Supercapacitors. Chemistry - A European Journal, 2014, 20, 564-574.	3.3	388

#	Article	IF	CITATIONS
19	A Stable Bifunctional Catalyst for Rechargeable Zinc–Air Batteries: Iron–Cobalt Nanoparticles Embedded in a Nitrogenâ€Doped 3D Carbon Matrix. Angewandte Chemie - International Edition, 2018, 57, 16166-16170.	13.8	365
20	A Promoted Charge Separation/Transfer System from Cu Single Atoms and C ₃ N ₄ Layers for Efficient Photocatalysis. Advanced Materials, 2020, 32, e2003082.	21.0	333
21	Operando Cooperated Catalytic Mechanism of Atomically Dispersed Cuâ^'N ₄ and Znâ^'N ₄ for Promoting Oxygen Reduction Reaction. Angewandte Chemie - International Edition, 2021, 60, 14005-14012.	13.8	312
22	Preparation and Characterization of Stable Biphase TiO ₂ Photocatalyst with High Crystallinity, Large Surface Area, and Enhanced Photoactivity. Journal of Physical Chemistry C, 2008, 112, 3083-3089.	3.1	288
23	Longâ€Lived, Visibleâ€Lightâ€Excited Charge Carriers of TiO ₂ /BiVO ₄ Nanocomposites and their Unexpected Photoactivity for Water Splitting. Advanced Energy Materials, 2014, 4, 1300995.	19.5	268
24	Porous Graphitic Carbon Nanosheets Derived from Cornstalk Biomass for Advanced Supercapacitors. ChemSusChem, 2013, 6, 880-889.	6.8	257
25	3D hierarchical flower-like TiO2 nanostructure: morphology control and its photocatalytic property. CrystEngComm, 2011, 13, 2994.	2.6	237
26	Hierarchical MoS2/Bi2MoO6 composites with synergistic effect for enhanced visible photocatalytic activity. Applied Catalysis B: Environmental, 2015, 164, 40-47.	20.2	237
27	An effective strategy for small-sized and highly-dispersed palladium nanoparticles supported on graphene with excellent performance for formic acid oxidation. Journal of Materials Chemistry, 2011, 21, 3384.	6.7	235
28	Ultrathin Porous Carbon Nitride Bundles with an Adjustable Energy Band Structure toward Simultaneous Solar Photocatalytic Water Splitting and Selective Phenylcarbinol Oxidation. Angewandte Chemie - International Edition, 2021, 60, 4815-4822.	13.8	233
29	Twoâ€Dimensional Porous Molybdenum Phosphide/Nitride Heterojunction Nanosheets for pHâ€Universal Hydrogen Evolution Reaction. Angewandte Chemie - International Edition, 2021, 60, 6673-6681.	13.8	227
30	Enhanced Photocatalytic Activity and Electron Transfer Mechanisms of Graphene/TiO ₂ with Exposed {001} Facets. Journal of Physical Chemistry C, 2011, 115, 23718-23725.	3.1	223
31	Exceptional Visibleâ€Lightâ€Driven Cocatalystâ€Free Photocatalytic Activity of gâ€C ₃ N ₄ by Well Designed Nanocomposites with Plasmonic Au and SnO ₂ . Advanced Energy Materials, 2016, 6, 1601190.	19.5	207
32	Effect of surface species on Cu-TiO2 photocatalytic activity. Applied Surface Science, 2008, 254, 2569-2574.	6.1	201
33	Facile strategy for controllable synthesis of stable mesoporous black TiO ₂ hollow spheres with efficient solar-driven photocatalytic hydrogen evolution. Journal of Materials Chemistry A, 2016, 4, 7495-7502.	10.3	198
34	Trapping [PMo ₁₂ O ₄₀] ^{3â^`} clusters into pre-synthesized ZIF-67 toward Mo _x Co _x C particles confined in uniform carbon polyhedrons for efficient overall water splitting. Chemical Science, 2018, 9, 4746-4755.	7.4	189
35	Porous NiCoP nanosheets as efficient and stable positive electrodes for advanced asymmetric supercapacitors. Journal of Materials Chemistry A, 2018, 6, 17905-17914.	10.3	189
36	Defects-engineering of magnetic γ-Fe2O3 ultrathin nanosheets/mesoporous black TiO2 hollow sphere heterojunctions for efficient charge separation and the solar-driven photocatalytic mechanism of tetracycline degradation. Applied Catalysis B: Environmental, 2019, 240, 319-328.	20.2	188

#	Article	IF	CITATIONS
37	NiSeâ€Ni _{0.85} Se Heterostructure Nanoflake Arrays on Carbon Paper as Efficient Electrocatalysts for Overall Water Splitting. Small, 2018, 14, e1800763.	10.0	185
38	Hierarchical Core–Shell Carbon Nanofiber@ZnIn ₂ S ₄ Composites for Enhanced Hydrogen Evolution Performance. ACS Applied Materials & Interfaces, 2014, 6, 13841-13849.	8.0	179
39	Facile preparation of porous NiTiO3 nanorods with enhanced visible-light-driven photocatalytic performance. Journal of Materials Chemistry, 2012, 22, 16471.	6.7	176
40	Cubic quantum dot/hexagonal microsphere ZnIn ₂ S ₄ heterophase junctions for exceptional visible-light-driven photocatalytic H ₂ evolution. Journal of Materials Chemistry A, 2017, 5, 8451-8460.	10.3	176
41	Phosphorusâ€Doped Carbon Nitride Tubes with a Layered Microâ€nanostructure for Enhanced Visibleâ€Light Photocatalytic Hydrogen Evolution. Angewandte Chemie, 2016, 128, 1862-1866.	2.0	173
42	Synthesis and photocatalytic activity of stable nanocrystalline TiO2 with high crystallinity and large surface area. Journal of Hazardous Materials, 2009, 161, 1122-1130.	12.4	172
43	In situ controlled growth of ZnIn2S4 nanosheets on reduced graphene oxide for enhanced photocatalytic hydrogen production performance. Chemical Communications, 2013, 49, 2237.	4.1	171
44	A highly active oxygen evolution electrocatalyst: Ultrathin CoNi double hydroxide/CoO nanosheets synthesized via interface-directed assembly. Nano Research, 2016, 9, 713-725.	10.4	171
45	Facile synthesis of sheet-like ZnO assembly composed of small ZnO particles for highly efficient photocatalysis. Journal of Materials Chemistry A, 2013, 1, 5700.	10.3	170
46	Defect-mediated electron–hole separation in semiconductor photocatalysis. Inorganic Chemistry Frontiers, 2018, 5, 1240-1254.	6.0	166
47	Highly concentrated, stable nitrogen-doped graphene for supercapacitors: Simultaneous doping and reduction. Applied Surface Science, 2012, 258, 3438-3443.	6.1	163
48	Co ₃ O ₄ nanocrystal ink printed on carbon fiber paper as a large-area electrode for electrochemical water splitting. Chemical Communications, 2015, 51, 8066-8069.	4.1	163
49	Photoinduced charge property of nanosized perovskite-type LaFeO3 and its relationships with photocatalytic activity under visible irradiation. Materials Research Bulletin, 2007, 42, 203-212.	5.2	162
50	Hierarchical MoS ₂ @MoP core–shell heterojunction electrocatalysts for efficient hydrogen evolution reaction over a broad pH range. Nanoscale, 2016, 8, 11052-11059.	5.6	160
51	A facile one-pot route for the controllable growth of small sized and well-dispersed ZnO particles on GO-derived graphene. Journal of Materials Chemistry, 2012, 22, 11778.	6.7	159
52	Sequential two-step hydrothermal growth of MoS2/CdS core-shell heterojunctions for efficient visible light-driven photocatalytic H2 evolution. Applied Catalysis B: Environmental, 2017, 203, 955-963.	20.2	159
53	Dynamics of photogenerated charges in the phosphate modified TiO2 and the enhanced activity for photoelectrochemical water splitting. Energy and Environmental Science, 2012, 5, 6552.	30.8	143
54	Exceptional Photocatalytic Activity of 001-Facet-Exposed TiO ₂ Mainly Depending on Enhanced Adsorbed Oxygen by Residual Hydrogen Fluoride. ACS Catalysis, 2013, 3, 1378-1385.	11.2	137

#	Article	IF	CITATIONS
55	In Situ Growth of TiO ₂ in Interlayers of Expanded Graphite for the Fabrication of TiO ₂ –Graphene with Enhanced Photocatalytic Activity. Chemistry - A European Journal, 2011, 17, 8379-8387.	3.3	135
56	Enhanced Visible Activities of α-Fe ₂ O ₃ by Coupling N-Doped Graphene and Mechanism Insight. ACS Catalysis, 2014, 4, 990-998.	11.2	132
57	<i>In Situ</i> Carbon-Coated Yolk–Shell V ₂ O ₃ Microspheres for Lithium-Ion Batteries. ACS Applied Materials & Interfaces, 2015, 7, 1595-1601.	8.0	132
58	Study on the mechanisms of photoinduced carriers separation and recombination for Fe3+–TiO2 photocatalysts. Applied Surface Science, 2007, 253, 4390-4395.	6.1	131
59	Carbothermal synthesis of ordered mesoporous carbon-supported nano zero-valent iron with enhanced stability and activity for hexavalent chromium reduction. Journal of Hazardous Materials, 2016, 309, 249-258.	12.4	131
60	A "MOFs plus MOFs―strategy toward Co–Mo ₂ N tubes for efficient electrocatalytic overall water splitting. Journal of Materials Chemistry A, 2018, 6, 20100-20109.	10.3	131
61	Small-sized and high-dispersed WN from [SiO ₄ (W ₃ O ₉ 1 ₄] ^{4â^'} clusters loading on GO-derived graphene as promising carriers for methanol electro-oxidation. Energy and Environmental Science, 2014, 7, 1939-1949.	30.8	130
62	Facile synthesis of novel 3D nanoflower-like CuxO/multilayer graphene composites for room temperature NOx gas sensor application. Nanoscale, 2014, 6, 7369.	5.6	130
63	Interconnected 1D Co3O4 nanowires on reduced graphene oxide for enzymeless H2O2 detection. Nano Research, 2015, 8, 469-480.	10.4	129
64	Isolated Boron and Nitrogen Sites on Porous Graphitic Carbon Synthesized from Nitrogenâ€Containing Chitosan for Supercapacitors. ChemSusChem, 2014, 7, 1637-1646.	6.8	128
65	Construction of Sixâ€Oxygenâ€Coordinated Single Ni Sites on gâ€C ₃ N ₄ with Boronâ€Oxo Species for Photocatalytic Waterâ€Activationâ€Induced CO ₂ Reduction. Advanced Materials, 2021, 33, e2105482.	21.0	128
66	Mass Production of Graphene via an in Situ Self-Generating Template Route and Its Promoted Activity as Electrocatalytic Support for Methanol Electroxidization. Journal of Physical Chemistry C, 2010, 114, 8727-8733.	3.1	127
67	Facile Synthesis of High-Crystallinity Graphitic Carbon/Fe ₃ C Nanocomposites As Counter Electrodes for High-Efficiency Dye-Sensitized Solar Cells. ACS Applied Materials & Interfaces, 2013, 5, 3663-3670.	8.0	127
68	Mesoporous TiO ₂ : Preparation, Doping, and as a Composite for Photocatalysis. ChemCatChem, 2013, 5, 885-894.	3.7	126
69	Effects of Cr-doping on the photoluminescence and ferromagnetism at room temperature in ZnO nanomaterials prepared by soft chemistry route. Materials Chemistry and Physics, 2009, 113, 103-106.	4.0	123
70	Visible‣ight Responsive TiO ₂ â€Based Materials for Efficient Solar Energy Utilization. Advanced Energy Materials, 2021, 11, 2003303.	19.5	118
71	Mesoporous SiO ₂ -Modified Nanocrystalline TiO ₂ with High Anatase Thermal Stability and Large Surface Area as Efficient Photocatalyst. Journal of Physical Chemistry C, 2009, 113, 1006-1013.	3.1	117
72	lon-exchanged route synthesis of Fe2N–N-doped graphitic nanocarbons composite as advanced oxygen reduction electrocatalyst. Chemical Communications, 2013, 49, 3022.	4.1	116

#	Article	IF	CITATIONS
73	Synthesis of large surface area LaFeO3 nanoparticles by SBA-16 template method as high active visible photocatalysts. Journal of Nanoparticle Research, 2010, 12, 967-974.	1.9	112
74	Hierarchical composites of TiO2 nanowire arrays on reduced graphene oxide nanosheets with enhanced photocatalytic hydrogen evolution performance. Journal of Materials Chemistry A, 2014, 2, 4366-4374.	10.3	112
75	Synergistic Effect of Tungsten Carbide and Palladium on Graphene for Promoted Ethanol Electrooxidation. ACS Applied Materials & Interfaces, 2013, 5, 6571-6579.	8.0	108
76	Mesoporous TiO ₂ /α-Fe ₂ O ₃ : Bifunctional Composites for Effective Elimination of Arsenite Contamination through Simultaneous Photocatalytic Oxidation and Adsorption. Journal of Physical Chemistry C, 2008, 112, 19584-19589.	3.1	107
77	Luminescence Functionalization of SBA-15 by YVO4:Eu3+as a Novel Drug Delivery System. Inorganic Chemistry, 2007, 46, 3203-3211.	4.0	106
78	Hierarchical CuS hollow nanospheres and their structure-enhanced visible light photocatalytic properties. CrystEngComm, 2013, 15, 5144.	2.6	106
79	Hierarchical flake-like Bi2MoO6/TiO2 bilayer films for visible-light-induced self-cleaning applications. Journal of Materials Chemistry A, 2013, 1, 6961.	10.3	102
80	Composites of small Ag clusters confined in the channels of well-ordered mesoporous anatase TiO2 and their excellent solar-light-driven photocatalytic performance. Nano Research, 2014, 7, 731-742.	10.4	102
81	Cluster-like molybdenum phosphide anchored on reduced graphene oxide for efficient hydrogen evolution over a broad pH range. Chemical Communications, 2016, 52, 9530-9533.	4.1	102
82	Self-floating amphiphilic black TiO2 foams with 3D macro-mesoporous architectures as efficient solar-driven photocatalysts. Applied Catalysis B: Environmental, 2017, 206, 336-343.	20.2	102
83	Enhanced photocatalytic activity of S-doped TiO2–ZrO2 nanoparticles under visible-light irradiation. Journal of Hazardous Materials, 2009, 166, 939-944.	12.4	101
84	3D hierarchical V–Ni-based nitride heterostructure as a highly efficient pH-universal electrocatalyst for the hydrogen evolution reaction. Journal of Materials Chemistry A, 2019, 7, 15823-15830.	10.3	100
85	Growth of small sized CeO2 particles in the interlayers of expanded graphite for high-performance room temperature NOx gas sensors. Journal of Materials Chemistry A, 2013, 1, 12742.	10.3	96
86	Graphene Quantumâ€Dotâ€Modified Hexagonal Tubular Carbon Nitride for Visibleâ€Light Photocatalytic Hydrogen Evolution. ChemCatChem, 2018, 10, 1330-1335.	3.7	95
87	Alumina decorated TiO2 nanotubes with ordered mesoporous walls as high sensitivity NOx gas sensors at room temperature. Nanoscale, 2013, 5, 8569.	5.6	94
88	In situ synthesis of a NiS/Ni ₃ S ₂ nanorod composite array on Ni foil as a FTO-free counter electrode for dye-sensitized solar cells. Nanoscale, 2015, 7, 1623-1626.	5.6	94
89	Magnetic Fe2O3/mesoporous black TiO2 hollow sphere heterojunctions with wide-spectrum response and magnetic separation. Applied Catalysis B: Environmental, 2018, 221, 235-242.	20.2	92
90	Structural Design Strategy and Active Site Regulation of Highâ€Efficient Bifunctional Oxygen Reaction Electrocatalysts for Zn–Air Battery. Small, 2021, 17, e2006766.	10.0	89

#	Article	IF	CITATIONS
91	Preparation of Large-Pore Mesoporous Nanocrystalline TiO2 Thin Films with Tailored Pore Diameters. Journal of Physical Chemistry B, 2005, 109, 18719-18722.	2.6	87
92	Synthesis of nanocrystalline anatase TiO2 by one-pot two-phase separated hydrolysis-solvothermal processes and its high activity for photocatalytic degradation of rhodamine B. Journal of Hazardous Materials, 2010, 176, 139-145.	12.4	87
93	Strongly coupled Ag/TiO2 heterojunctions for effective and stable photothermal catalytic reduction of 4-nitrophenol. Nano Research, 2018, 11, 126-141.	10.4	87
94	A hierarchical porous carbon material from a loofah sponge network for high performance supercapacitors. RSC Advances, 2015, 5, 42430-42437.	3.6	86
95	Effective Electrocatalytic Hydrogen Evolution in Neutral Medium Based on 2D MoP/MoS ₂ Heterostructure Nanosheets. ACS Applied Materials & Interfaces, 2019, 11, 25986-25995.	8.0	86
96	Magnetically separable porous graphitic carbon with large surface area as excellent adsorbents for metal ions and dye. Journal of Materials Chemistry, 2011, 21, 7232.	6.7	85
97	Vanadiumâ€Incorporated CoP ₂ with Lattice Expansion for Highly Efficient Acidic Overall Water Splitting. Angewandte Chemie - International Edition, 2022, 61, .	13.8	85
98	Controlled synthesis of thorny anatase TiO ₂ tubes for construction of Ag–AgBr/TiO ₂ composites as highly efficient simulated solar-light photocatalyst. Journal of Materials Chemistry, 2012, 22, 2081-2088.	6.7	84
99	Smallâ€Sized and Contacting Pt–WC Nanostructures on Graphene as Highly Efficient Anode Catalysts for Direct Methanol Fuel Cells. Chemistry - A European Journal, 2012, 18, 7443-7451.	3.3	83
100	A novel soft template strategy to fabricate mesoporous carbon/graphene composites as high-performance supercapacitor electrodes. RSC Advances, 2012, 2, 8359.	3.6	82
101	Porous Cobalt Titanate Nanorod: A New Candidate for Visible Lightâ€Driven Photocatalytic Water Oxidation. ChemCatChem, 2014, 6, 265-270.	3.7	81
102	Selective Hydrogenation of Cinnamaldehyde to Cinnamal Alcohol over Platinum/Graphene Catalysts. ChemCatChem, 2014, 6, 3246-3253.	3.7	80
103	In situ growth of Bi ₂ MoO ₆ on reduced graphene oxide nanosheets for improved visible-light photocatalytic activity. CrystEngComm, 2014, 16, 842-849.	2.6	80
104	Relationships of surface oxygen vacancies with photoluminescence and photocatalytic performance of ZnO nanoparticles. Science in China Series B: Chemistry, 2005, 48, 25-30.	0.8	79
105	Bifunctional Ag/Fe/N/C Catalysts for Enhancing Oxygen Reduction via Cathodic Biofilm Inhibition in Microbial Fuel Cells. ACS Applied Materials & amp; Interfaces, 2016, 8, 6992-7002.	8.0	78
106	Co-vacancy-rich Co1–x S nanosheets anchored on rGO for high-efficiency oxygen evolution. Nano Research, 2017, 10, 1819-1831.	10.4	78
107	Assembly of TiO2 ultrathin nanosheets with surface lattice distortion for solar-light-driven photocatalytic hydrogen evolution. Applied Catalysis B: Environmental, 2018, 239, 317-323.	20.2	77
108	From graphite to porous graphene-like nanosheets for high rate lithium-ion batteries. Nano Research, 2015, 8, 2998-3010.	10.4	76

#	Article	IF	CITATIONS
109	Enhanced photogenerated carrier separation in CdS quantum dot sensitized ZnFe ₂ O ₄ /ZnIn ₂ S ₄ nanosheet stereoscopic films for exceptional visible light photocatalytic H ₂ evolution performance. Nanoscale, 2017, 9, 5912-5921.	5.6	76
110	Small-sized tungsten nitride anchoring into a 3D CNT-rGO framework as a superior bifunctional catalyst for the methanol oxidation and oxygen reduction reactions. Nano Research, 2016, 9, 329-343.	10.4	75
111	Dual-valence nickel nanosheets covered with thin carbon as bifunctional electrocatalysts for full water splitting. Journal of Materials Chemistry A, 2016, 4, 7297-7304.	10.3	73
112	Assembly of β-Cyclodextrins Acting as Molecular Bricks onto Multiwall Carbon Nanotubes. Journal of Physical Chemistry C, 2008, 112, 951-957.	3.1	72
113	Co–VN encapsulated in bamboo-like N-doped carbon nanotubes for ultrahigh-stability of oxygen reduction reaction. Nanoscale, 2018, 10, 4311-4319.	5.6	72
114	Ni ₃ S ₂ Nanosheets in Situ Epitaxially Grown on Nanorods as High Active and Stable Homojunction Electrocatalyst for Hydrogen Evolution Reaction. ACS Sustainable Chemistry and Engineering, 2018, 6, 2474-2481.	6.7	72
115	Hierarchical whisker-on-sheet NiCoP with adjustable surface structure for efficient hydrogen evolution reaction. Nanoscale, 2018, 10, 7619-7629.	5.6	72
116	Highâ€Efficient, Stable Electrocatalytic Hydrogen Evolution in Acid Media by Amorphous Fe <i>_x</i> P Coating Fe ₂ N Supported on Reduced Graphene Oxide. Small, 2018, 14, e1801717.	10.0	72
117	Highly crystalline, small sized, monodisperse α-NiS nanocrystal ink as an efficient counter electrode for dye-sensitized solar cells. Journal of Materials Chemistry A, 2015, 3, 15905-15912.	10.3	69
118	GO-induced assembly of gelatin toward stacked layer-like porous carbon for advanced supercapacitors. Nanoscale, 2016, 8, 2418-2427.	5.6	69
119	Inorganic acid-derived hydrogen-bonded organic frameworks to form nitrogen-rich carbon nitrides for photocatalytic hydrogen evolution. Journal of Materials Chemistry A, 2017, 5, 21979-21985.	10.3	69
120	B and N isolate-doped graphitic carbon nanosheets from nitrogen-containing ion-exchanged resins for enhanced oxygen reduction. Scientific Reports, 2014, 4, 5184.	3.3	68
121	Nitrogen-doped graphene supported Pd@PdO core-shell clusters for C-C coupling reactions. Nano Research, 2014, 7, 1280-1290.	10.4	66
122	Exceptional visible-light photoelectrocatalytic activity of In2O3/In2S3/CdS ternary stereoscopic porous heterostructure film for the degradation of persistent 4-fluoro-3-methylphenol. Applied Catalysis B: Environmental, 2018, 225, 477-486.	20.2	66
123	A dual-active Co-CoO heterojunction coupled with Ti3C2-MXene for highly-performance overall water splitting. Nano Research, 2022, 15, 238-247.	10.4	66
124	Engineering oxygen vacancy on rutile TiO2 for efficient electron-hole separation and high solar-driven photocatalytic hydrogen evolution. Science China Materials, 2018, 61, 822-830.	6.3	65
125	CoO-Mo2N hollow heterostructure for high-efficiency electrocatalytic hydrogen evolution reaction. NPG Asia Materials, 2019, 11, .	7.9	65
126	Co ₃ O ₄ nanosheets as a high-performance catalyst for oxygen evolution proceeding via a double two-electron process. Chemical Communications, 2016, 52, 6705-6708.	4.1	64

#	Article	IF	CITATIONS
127	A Stable Bifunctional Catalyst for Rechargeable Zinc–Air Batteries: Iron–Cobalt Nanoparticles Embedded in a Nitrogenâ€Doped 3D Carbon Matrix. Angewandte Chemie, 2018, 130, 16398-16402.	2.0	64
128	CoSe ₂ /N-Doped Carbon Hybrid Derived from ZIF-67 as High-Efficiency Counter Electrode for Dye-Sensitized Solar Cells. ACS Sustainable Chemistry and Engineering, 2019, 7, 2784-2791.	6.7	64
129	NaYF4:Er3+/Yb3+–graphene composites: preparation, upconversion luminescence, and application in dye-sensitized solar cells. Journal of Materials Chemistry, 2012, 22, 20381.	6.7	63
130	N-Doped carbon coating enhances the bifunctional oxygen reaction activity of CoFe nanoparticles for a highly stable Zn–air battery. Journal of Materials Chemistry A, 2020, 8, 21189-21198.	10.3	63
131	Electronic Tuning of Ni by Mo Species for Highly Efficient Hydroisomerization of <i>n</i> -Alkanes Comparable to Pt-Based Catalysts. ACS Catalysis, 2020, 10, 10449-10458.	11.2	63
132	Synthesis of High-Activity TiO ₂ -Based Photocatalysts by Compounding a Small Amount of Porous Nanosized LaFeO ₃ and the Activity-Enhanced Mechanisms. Journal of Physical Chemistry C, 2011, 115, 12375-12380.	3.1	62
133	Preparation of La-Mn-O Perovskite Catalyst by Microwave Irradiation Method and its Application to Methane Combustion. Catalysis Letters, 2010, 135, 152-158.	2.6	61
134	Synergetic enhancement of surface reactions and charge separation over holey C3N4/TiO2 2D heterojunctions. Science Bulletin, 2021, 66, 275-283.	9.0	61
135	A Floating Porous Crystalline TiO ₂ Ceramic with Enhanced Photocatalytic Performance for Wastewater Decontamination. European Journal of Inorganic Chemistry, 2013, 2013, 2411-2417.	2.0	59
136	Hierarchical Composite of Ag/AgBr Nanoparticles Supported on Bi ₂ MoO ₆ Hollow Spheres for Enhanced Visible‣ight Photocatalytic Performance. ChemPlusChem, 2013, 78, 117-123.	2.8	58
137	Synergistic effect of Mo ₂ N and Pt for promoted selective hydrogenation of cinnamaldehyde over Pt–Mo ₂ N/SBA-15. Catalysis Science and Technology, 2016, 6, 2403-2412.	4.1	58
138	Novel heterogeneous CdS nanoparticles/NiTiO3 nanorods with enhanced visible-light-driven photocatalytic activity. RSC Advances, 2013, 3, 18305.	3.6	56
139	Porous cobalt/tungsten nitride polyhedra as efficient bifunctional electrocatalysts for overall water splitting. Journal of Materials Chemistry A, 2020, 8, 22938-22946.	10.3	56
140	In situ simultaneous synthesis of WC/graphitic carbon nanocomposite as a highly efficient catalyst support for DMFC. Chemical Communications, 2009, , 3104.	4.1	55
141	Zinc assisted epitaxial growth of N-doped CNTs-based zeolitic imidazole frameworks derivative for high efficient oxygen reduction reaction in Zn-air battery. Chemical Engineering Journal, 2021, 414, 127569.	12.7	55
142	Inâ€Situ Fabrication of Ag/Ag ₃ PO ₄ /Graphene Triple Heterostructure Visibleâ€Light Photocatalyst through Grapheneâ€Assisted Reduction Strategy. ChemCatChem, 2013, 5, 1359-1367.	3.7	54
143	Synergism of molybdenum nitride and palladium for high-efficiency formic acid electrooxidation. Journal of Materials Chemistry A, 2018, 6, 7623-7630.	10.3	54
144	Superhydrophilic anatase TiO2 film with the micro- and nanometer-scale hierarchical surface structure. Materials Letters, 2008, 62, 3503-3505.	2.6	53

#	Article	IF	CITATIONS
145	Lowâ€Pt Loaded on a Vanadium Nitride/Graphitic Carbon Composite as an Efficient Electrocatalyst for the Oxygen Reduction Reaction. Chemistry - A European Journal, 2013, 19, 13979-13986.	3.3	53
146	In situ formation of a ZnO/ZnSe nanonail array as a photoelectrode for enhanced photoelectrochemical water oxidation performance. Nanoscale, 2016, 8, 9366-9375.	5.6	52
147	Cobalt-vanadium bimetal-based nanoplates for efficient overall water splitting. Science China Materials, 2018, 61, 80-90.	6.3	52
148	Cubic imidazolate frameworks-derived CoFe alloy nanoparticles-embedded N-doped graphitic carbon for discharging reaction of Zn-air battery. Science China Materials, 2020, 63, 327-338.	6.3	51
149	Single Metal Atom Decorated Carbon Nitride for Efficient Photocatalysis: Synthesis, Structure, and Applications. Solar Rrl, 2021, 5, 2000609.	5.8	51
150	Controlled Atmosphere Corrosion Engineering toward Inhomogeneous NiFe-LDH for Energetic Oxygen Evolution. ACS Nano, 2022, 16, 7794-7803.	14.6	51
151	Multivalent Sn species synergistically favours the CO2-into-HCOOH conversion. Nano Research, 2021, 14, 1053-1060.	10.4	49
152	B,N-Doped Defective Carbon Entangled Fe ₃ C Nanoparticles as the Superior Oxygen Reduction Electrocatalyst for Zn–Air Batteries. ACS Sustainable Chemistry and Engineering, 2019, 7, 19104-19112.	6.7	48
153	Recent advances of biomass derived carbon-based materials for efficient electrochemical energy devices. Journal of Materials Chemistry A, 2022, 10, 9277-9307.	10.3	48
154	Unraveling the mechanism for paired electrocatalysis of organics with water as a feedstock. Nature Communications, 2022, 13, .	12.8	48
155	A chromium nitride/carbon nitride containing graphitic carbon nanocapsule hybrid as a Pt-free electrocatalyst for oxygen reduction. Chemical Communications, 2015, 51, 12399-12402.	4.1	46
156	Porous Plate-like MoP Assembly as an Efficient pH-Universal Hydrogen Evolution Electrocatalyst. ACS Applied Materials & Interfaces, 2020, 12, 49596-49606.	8.0	46
157	A novel Fe ₃ C/graphitic carbon composite with electromagnetic wave absorption properties in the C-band. RSC Advances, 2015, 5, 60135-60140.	3.6	45
158	A Unique Fe–N ₄ Coordination System Enabling Transformation of Oxygen into Superoxide for Photocatalytic CH Activation with High Efficiency and Selectivity. Advanced Materials, 2022, 34, e2200612.	21.0	43
159	Threeâ€Dimensional Fe ₂ N@C Microspheres Grown on Reduced Graphite Oxide for Lithiumâ€Ion Batteries and the Li Storage Mechanism. Chemistry - A European Journal, 2015, 21, 3249-3256.	3.3	42
160	Porous NiCoP nanowalls as promising electrode with high-area and mass capacitance for supercapacitors. Science China Materials, 2019, 62, 1115-1126.	6.3	42
161	Efficiently photocatalytic degradation of monochlorophenol on in-situ fabricated BiPO4/β-Bi2O3 heterojunction microspheres and O2-free hole-induced selective dechloridation conversion with H2 evolution. Applied Catalysis B: Environmental, 2020, 263, 118313.	20.2	42
162	Co2Nx/nitrogen-doped reduced graphene oxide for enzymeless glucose detection. Chemical Communications, 2014, 50, 4921-4923.	4.1	41

#	Article	IF	CITATIONS
163	Vertical α-FeOOH nanowires grown on the carbon fiber paper as a free-standing electrode for sensitive H2O2 detection. Nano Research, 2016, 9, 2260-2269.	10.4	41
164	Recent advances in rechargeable Zn-based batteries. Journal of Power Sources, 2021, 493, 229677.	7.8	41
165	Nitrogen-self-doped graphene as a high capacity anode material for lithium-ion batteries. Journal of Materials Chemistry A, 2013, 1, 14586.	10.3	40
166	A novel Ag/graphene composite: facile fabrication and enhanced antibacterial properties. Journal of Materials Science, 2013, 48, 1980-1985.	3.7	40
167	Engineering a stereo-film of FeNi ₃ nanosheet-covered FeOOH arrays for efficient oxygen evolution. Nanoscale, 2018, 10, 10971-10978.	5.6	40
168	Carbon nanotubes <i>in situ</i> embedded with NiS nanocrystals outperform Pt in dye-sensitized solar cells: interface improved activity. Journal of Materials Chemistry A, 2019, 7, 10405-10411.	10.3	40
169	Urchin-like V ₂ O ₃ /C Hollow Nanosphere Hybrid for High-Capacity and Long-Cycle-Life Lithium Storage. ACS Sustainable Chemistry and Engineering, 2017, 5, 11238-11245.	6.7	39
170	Ni2P nanocrystals coated on carbon nanotubes as enhanced lightweight electromagnetic wave absorbers. Carbon, 2020, 161, 51-61.	10.3	39
171	Designed Synthesis and Catalytic Mechanisms of Nonâ€Precious Metal Singleâ€Atom Catalysts for Oxygen Reduction Reaction. Small Methods, 2021, 5, e2100865.	8.6	39
172	Room temperature solution synthesis of hierarchical bow-like Cu2O with high visible light driven photocatalytic activity. RSC Advances, 2012, 2, 2875.	3.6	38
173	One-step synthesis of a hierarchical Bi ₂ S ₃ nanoflowerIn ₂ S ₃ nanosheet composite with efficient visible-light photocatalytic activity. CrystEngComm, 2015, 17, 8720-8727.	2.6	38
174	Hexagonal FeS nanosheets with high-energy (001) facets: Counter electrode materials superior to platinum for dye-sensitized solar cells. Nano Research, 2016, 9, 2862-2874.	10.4	38
175	In situ synthesis, enhanced luminescence and application in dye sensitized solar cells of Y2O3/Y2O2S:Eu3+ nanocomposites by reduction of Y2O3:Eu3+. Scientific Reports, 2016, 6, 37133.	3.3	38
176	CoSe _x nanocrystalline-dotted CoCo layered double hydroxide nanosheets: a synergetic engineering process for enhanced electrocatalytic water oxidation. Nanoscale, 2017, 9, 16256-16263.	5.6	38
177	A facile route to carbide-based electrocatalytic nanocomposites. Journal of Materials Chemistry, 2012, 22, 5072.	6.7	37
178	Efficient photodecomposition of 2,4-dichlorophenol on recyclable phase-mixed hierarchically structured Bi ₂ O ₃ coupled with phosphate-bridged nano-SnO ₂ . Environmental Science: Nano, 2017, 4, 1147-1154.	4.3	37
179	One-Pot Synthesis and Characterization of Cu-SBA-16 Mesoporous Molecular Sieves as an Excellent Catalyst for Phenol Hydroxylation. Catalysis Letters, 2011, 141, 242-250.	2.6	36
180	Heterophase engineering of SnO2/Sn3O4 drives enhanced carbon dioxide electrocatalytic reduction to formic acid. Science China Materials, 2020, 63, 2314-2324.	6.3	36

#	Article	IF	CITATIONS
181	One-dimensional CO9S8-V3S4 heterojunctions as bifunctional electrocatalysts for highly efficient overall water splitting. Science China Materials, 2021, 64, 1396-1407.	6.3	36
182	Synthesis and applications of graphite carbon sphere with uniformly distributed magnetic Fe3O4 nanoparticles (MGCSs) and MGCS@Ag, MGCS@TiO2. Journal of Materials Chemistry, 2010, 20, 4802.	6.7	35
183	Highly dispersed Ni-decorated porous hollow carbon nanofibers: fabrication, characterization, and NOx gas sensors at room temperature. Journal of Materials Chemistry, 2012, 22, 24814.	6.7	35
184	Improved visible-light activities of nanocrystalline CdS by coupling with ultrafine NbN with lattice matching for hydrogen evolution. Sustainable Energy and Fuels, 2018, 2, 549-552.	4.9	35
185	ZnO-dotted porous ZnS cluster microspheres for high efficient, Pt-free photocatalytic hydrogen evolution. Scientific Reports, 2015, 5, 8858.	3.3	34
186	Ni ₂ P Entwined by Graphite Layers as a Low-Pt Electrocatalyst in Acidic Media for Oxygen Reduction. ACS Applied Materials & Interfaces, 2018, 10, 9999-10010.	8.0	34
187	N-doped carbon-coated Co3O4 nanosheet array/carbon cloth for stable rechargeable Zn-air batteries. Science China Materials, 2019, 62, 624-632.	6.3	34
188	Trace Pt Clusters Dispersed on SAPOâ€11 Promoting the Synergy of Metal Sites with Acid Sites for Highâ€Effective Hydroisomerization of <i>n</i> â€Alkanes. Small Methods, 2019, 3, 1800510.	8.6	34
189	Design and construction of Co3O4/PEl–CNTs composite exhibiting fast responding CO sensor at room temperature. CrystEngComm, 2013, 15, 4730.	2.6	33
190	Selenization of Cu ₂ ZnSnS ₄ Enhanced the Performance of Dye-Sensitized Solar Cells: Improved Zinc-Site Catalytic Activity for I ₃ [–] . ACS Applied Materials & Interfaces, 2017, 9, 37662-37670.	8.0	33
191	2-D porous Ni ₃ N–Co ₃ N hybrids derived from ZIF-67/Ni(OH) ₂ sheets as a magnetically separable catalyst for hydrogenation reactions. Chemical Communications, 2018, 54, 11088-11091.	4.1	33
192	Hydrogenated TiO2/SrTiO3 porous microspheres with tunable band structure for solar-light photocatalytic H2 and O2 evolution. Science China Materials, 2016, 59, 1003-1016.	6.3	32
193	Hierarchical porous NiCo ₂ O ₄ nanosheet arrays directly grown on carbon cloth with superior lithium storage performance. Dalton Transactions, 2017, 46, 4717-4723.	3.3	32
194	One-pot Hydrothermal Synthesis of Mesoporous V-SBA-16 with a Function of the pH of the Initial Gel and its Improved Catalytic Performance for Benzene Hydroxylation. Catalysis Letters, 2012, 142, 619-626.	2.6	31
195	Fabrication of mixed-crystalline-phase spindle-like TiO2 for enhanced photocatalytic hydrogen production. Science China Materials, 2015, 58, 363-369.	6.3	31
196	Hollow CoP spheres assembled from porous nanosheets as high-rate and ultra-stable electrodes for advanced supercapacitors. Journal of Materials Chemistry A, 2021, 9, 26226-26235.	10.3	31
197	Synthesis of Pd on porous hollow carbon spheres as an electrocatalyst for alcohol electrooxidation. RSC Advances, 2011, 1, 191.	3.6	30
198	Facile Synthesis of Porous Zn ₂ Ti ₃ O ₈ Nanorods for Photocatalytic Overall Water Splitting. ChemCatChem, 2014, 6, 2258-2262.	3.7	30

#	Article	IF	CITATIONS
199	Hierarchical Nâ€Doped TiO ₂ Microspheres with Exposed (001) Facets for Enhanced Visible Light Catalysis. European Journal of Inorganic Chemistry, 2014, 2014, 2146-2152.	2.0	29
200	3D Network nanostructured NiCoP nanosheets supported on N-doped carbon coated Ni foam as a highly active bifunctional electrocatalyst for hydrogen and oxygen evolution reactions. Frontiers of Chemical Science and Engineering, 2018, 12, 417-424.	4.4	28
201	Ultra-small Mo ₂ N on SBA-15 as a highly efficient promoter of low-loading Pd for catalytic hydrogenation. Nanoscale, 2018, 10, 22348-22356.	5.6	28
202	Electronic Structure Modulation of Nonâ€Nobleâ€Metalâ€Based Catalysts for Biomass Electrooxidation Reactions. Small Structures, 2021, 2, 2100095.	12.0	28
203	Fabrication of a 3D Hierarchical Flowerâ€Like MgO Microsphere and Its Application as Heterogeneous Catalyst. European Journal of Inorganic Chemistry, 2012, 2012, 954-960.	2.0	27
204	Single-step pyrolytic preparation of Mo2C/graphitic carbon nanocomposite as catalyst carrier for the direct liquid-feed fuel cells. RSC Advances, 2013, 3, 4771.	3.6	27
205	Synergistic Effect of Tungsten Nitride and Palladium for the Selective Hydrogenation of Cinnamaldehyde at the C=C bond. ChemCatChem, 2016, 8, 1718-1726.	3.7	26
206	Solar-boosted electrocatalytic oxygen evolution via catalytic site remodelling of CoCr layered double hydroxide. Applied Catalysis B: Environmental, 2021, 284, 119707.	20.2	26
207	A facile and green synthesis route towards two-dimensional TiO2@Ag heterojunction structure with enhanced visible light photocatalytic activity. CrystEngComm, 2013, 15, 5821.	2.6	25
208	Super-stable non-woven fabric-based membrane as a high-efficiency oil/water separator in full pH range. RSC Advances, 2017, 7, 19764-19770.	3.6	25
209	Twoâ€Dimensional Porous Molybdenum Phosphide/Nitride Heterojunction Nanosheets for pHâ€Universal Hydrogen Evolution Reaction. Angewandte Chemie, 2021, 133, 6747-6755.	2.0	25
210	Hierarchical Ag/Ag ₂ S/CuS Ternary Heterostructure Composite as an Efficient Visible‣ight Photocatalyst. ChemCatChem, 2015, 7, 1684-1690.	3.7	23
211	Self-supported Ni6MnO8 3D mesoporous nanosheet arrays with ultrahigh lithium storage properties and conversion mechanism by in-situ XAFS. Nano Research, 2017, 10, 263-275.	10.4	23
212	Atomically Dispersed Fe–N ₃ C Sites Induce Asymmetric Electron Structures to Afford Superior Oxygen Reduction Activity. Small, 2022, 18, e2201255.	10.0	23
213	Solvothermal Synthesis, Characterization, and Formation Mechanism of a Single‣ayer Anatase TiO ₂ Nanosheet with a Porous Structure. European Journal of Inorganic Chemistry, 2011, 2011, 754-760.	2.0	22
214	Surface curvature-confined strategy to ultrasmall nickel-molybdenum sulfide nanoflakes for highly efficient deep hydrodesulfurization. Nano Research, 2020, 13, 882-890.	10.4	22
215	Operando Cooperated Catalytic Mechanism of Atomically Dispersed Cuâ~'N 4 and Znâ~'N 4 for Promoting Oxygen Reduction Reaction. Angewandte Chemie, 2021, 133, 14124-14131.	2.0	22
216	Multi-touch cobalt phosphide-tungsten phosphide heterojunctions anchored on reduced graphene oxide boosting wide pH hydrogen evolution. Science China Materials, 2022, 65, 1225-1236.	6.3	21

#	Article	IF	CITATIONS
217	Research progress of Fe-N-C catalysts for the electrocatalytic oxygen reduction reaction. Science China Materials, 2022, 65, 1701-1722.	6.3	21
218	Silica direct evaporation: a size-controlled approach to SiC/carbon nanosheet composites as Pt catalyst supports for superior methanol electrooxidation. Journal of Materials Chemistry A, 2015, 3, 24139-24147.	10.3	20
219	Znâ€Doped Porous CoNiP Nanosheet Arrays as Efficient and Stable Bifunctional Electrocatalysts for Overall Water Splitting. Energy Technology, 2020, 8, 1901079.	3.8	20
220	Oneâ€pot synthesis of silver particle aggregation as highly active SERS substrate. Journal of Raman Spectroscopy, 2011, 42, 5-11.	2.5	19
221	Facile synthesis and shape control of Fe3O4 nanocrystals with good dispersion and stabilization. CrystEngComm, 2013, 15, 3366.	2.6	19
222	Intermittent microwave heating-promoted rapid fabrication of sheet-like Ag assemblies and small-sized Ag particles and their use as co-catalyst of ZnO for enhanced photocatalysis. Journal of Materials Chemistry A, 2014, 2, 3015.	10.3	19
223	A "competitive occupancy―strategy toward Co–N ₄ single-atom catalysts embedded in 2D TiN/rGO sheets for highly efficient and stable aromatic nitroreduction. Journal of Materials Chemistry A, 2020, 8, 4807-4815.	10.3	19
224	Ultrathin Porous Carbon Nitride Bundles with an Adjustable Energy Band Structure toward Simultaneous Solar Photocatalytic Water Splitting and Selective Phenylcarbinol Oxidation. Angewandte Chemie, 2021, 133, 4865-4872.	2.0	19
225	In Situ Reduction, Oxygen Etching, and Reduction Using Formic Acid: An Effective Strategy for Controllable Growth of Monodisperse Palladium Nanoparticles on Graphene. ChemPlusChem, 2012, 77, 301-307.	2.8	18
226	Morphology Effect of NiSe Hierarchical Microspheres on the Performance of Dye-Sensitized Solar Cells. ACS Applied Nano Materials, 2018, 1, 4900-4909.	5.0	18
227	Constructing Pd-N interactions in Pd/g-C3N4 to improve the charge dynamics for efficient photocatalytic hydrogen evolution. Nano Research, 2022, 15, 2928-2934.	10.4	18
228	First-principles study on negative thermal expansion of PbTiO3. Applied Physics Letters, 2013, 103, .	3.3	17
229	A 3D all-inorganic architecture based on the [H2W12O42]10â^' building block with different alkaline-earth metal linkers: crystal structures, surface photovoltage and photoluminescent properties. CrystEngComm, 2013, 15, 4721.	2.6	17
230	Single-crystalline Bi ₁₉ Br ₃ S ₂₇ nanorods with an efficiently improved photocatalytic activity. CrystEngComm, 2015, 17, 6120-6126.	2.6	17
231	Gelatin-assisted synthesis of ZnS hollow nanospheres: the microstructure tuning, formation mechanism and application for Pt-free photocatalytic hydrogen production. CrystEngComm, 2017, 19, 461-468.	2.6	17
232	Smallâ€ s ized Tungsten Nitride Particles Strongly Anchored on Carbon Nanotubes and their Use as Supports for Pt for Methanol Electroâ€oxidation. Chemistry - A European Journal, 2015, 21, 18345-18353.	3.3	16
233	Insight on the active sites of CoNi alloy embedded in N-doped carbon nanotubes for oxygen reduction reaction. Science China Materials, 2021, 64, 2719-2728.	6.3	16
234	Vanadiumâ€Incorporated CoP ₂ with Lattice Expansion for Highly Efficient Acidic Overall Water Splitting. Angewandte Chemie, 2022, 134, .	2.0	16

#	Article	IF	CITATIONS
235	Fe3C coupled with Fe-Nx supported on N-doped carbon as oxygen reduction catalyst for assembling Zn-air battery to drive water splitting. Chinese Chemical Letters, 2022, 33, 3903-3908.	9.0	16
236	Heterojunction Ag–TiO ₂ Nanopillars for Visibleâ€Lightâ€Driven Photocatalytic H ₂ Production. ChemPlusChem, 2014, 79, 995-1000.	2.8	15
237	Surface domain heterojunction on rutile TiO ₂ for highly efficient photocatalytic hydrogen evolution. Nanoscale Horizons, 2020, 5, 1596-1602.	8.0	15
238	The Fe ₃ C–N _{<i>x</i>} Site Assists the Fe–N _{<i>x</i>} Site to Promote Activity of the Fe–N–C Electrocatalyst for Oxygen Reduction Reaction. ACS Sustainable Chemistry and Engineering, 2022, 10, 3346-3354.	6.7	15
239	Fabrication of noncovalently functionalized brick-like β-cyclodextrins/graphene composite dispersions with favorable stability. RSC Advances, 2014, 4, 2813-2819.	3.6	14
240	A Platinum–Vanadium Nitride/Porous Graphitic Nanocarbon Composite as an Excellent Catalyst for the Oxygen Reduction Reaction. ChemElectroChem, 2015, 2, 1813-1820.	3.4	14
241	Graphitic Carbon Nanocapsules: Scaled Preparation, Formation Mechanism, and Use as an Excellent Support for Methanol Electro-oxidation. European Journal of Inorganic Chemistry, 2012, 2012, 961-968.	2.0	13
242	Confinement Effect on Ag Clusters in the Channels of Wellâ€Ordered Mesoporous TiO ₂ and their Enhanced Photocatalytic Performance. ChemCatChem, 2013, 5, 1354-1358.	3.7	13
243	23327Enhanced photoelectric conversion efficiency of dye-sensitized solar cells by the incorporation of flower-like Bi2S3:Eu3+ sub-microspheres. Scientific Reports, 2016, 6, 23395.	3.3	13
244	Dyeâ€Sensitised Solar Cells Based on Largeâ€Pore Mesoporous TiO ₂ with Controllable Pore Diameters. European Journal of Inorganic Chemistry, 2011, 2011, 4730-4737.	2.0	12
245	A New Combustion Route to Synthesize Mixed Valence Vanadium Oxide Heterojunction Composites as Visibleâ€Lightâ€Driven Photocatalysts. ChemCatChem, 2014, 6, 2553-2559.	3.7	12
246	Constructing B and N separately co-doped carbon nanocapsules-wrapped Fe/Fe ₃ C for oxygen reduction reaction with high current density. Physical Chemistry Chemical Physics, 2016, 18, 26572-26578.	2.8	12
247	Porous Palladium Nanomeshes with Enhanced Electrochemical CO ₂ â€intoâ€Syngas Conversion over a Wider Applied Potential. ChemSusChem, 2019, 12, 3304-3311.	6.8	12
248	In situ intercalation and exploitation of Co3O4 nanoparticles grown on carbon nitride nanosheets for highly efficient degradation of methylene blue. Dalton Transactions, 2020, 49, 14665-14672.	3.3	12
249	Hydrothermal Synthesis of Cu@C Composite Spheres by a One‣tep Method and Their Use as Sacrificial Templates to Synthesize a CuO@SiO ₂ Core–Shell Structure. European Journal of Inorganic Chemistry, 2013, 2013, 4988-4997.	2.0	11
250	Preparation of KF–La ₂ O ₂ CO ₃ solid base catalysts and their excellent catalytic activities for transesterification of tributyrin with methanol. Catalysis Science and Technology, 2014, 4, 2957.	4.1	11
251	Facile One-Pot Method for the Synthesis of Novel N-Dichloroacetyl-1,3-oxazolidines. Synthetic Communications, 2009, 39, 2454-2463.	2.1	10
252	3 D Interlayer Nanohybrids Composed of Sulfamicâ€Acidâ€Doped PEdot Grown on Expanded Graphite for Highâ€Performance Supercapacitors. ChemPlusChem, 2016, 81, 242-250.	2.8	10

#	Article	IF	CITATIONS
253	Core–Shell NiO@Niâ€₽ Hybrid Nanosheet Array for Synergistically Enhanced Oxygen Evolution Electrocatalysis: Experimental and Theoretical Insights. Chemistry - an Asian Journal, 2018, 13, 944-949.	3.3	9
254	Supramolecular precursor derived loofah sponge-like Fe2Ox/C for effective synergistic reaction of Fenton and photocatalysis. Nano Research, 2022, 15, 1949-1958.	10.4	9
255	Advanced Research Progress on Highâ€Efficient Utilization of Pt Electrocatalysts in Fuel Cells. Energy Technology, 2021, 9, 2100227.	3.8	8
256	Ni-promoted MoS ₂ in hollow zeolite nanoreactors: enhanced catalytic activity and stability for deep hydrodesulfurization. Journal of Materials Chemistry A, 2022, 10, 7263-7270.	10.3	8
257	The confined growth of few-layered and ultrashort-slab Ni-promoted MoS2 on reduced graphene oxide for deep-degree hydrodesulfurization. Nano Research, 2022, 15, 7052-7062.	10.4	8
258	Functionalization of multi-walled carbon nanotube for electrocatalytic oxidation of nitric oxide. Journal of Applied Electrochemistry, 2010, 40, 593-599.	2.9	7
259	Preparation and characterization of chitosan microsphere loading bovine serum albumin. Journal Wuhan University of Technology, Materials Science Edition, 2012, 27, 459-464.	1.0	7
260	Freeâ€Standing Ultrathin Cobalt Nanosheets Synthesized by Means of In Situ Reduction and Interfaceâ€Directed Assembly and Their Magnetic Properties. ChemPlusChem, 2013, 78, 481-485.	2.8	6
261	A versatile salicylic acid precursor method for preparing titanate microspheres. Science China Materials, 2015, 58, 106-113.	6.3	6
262	Ni–Co Bimetallic Sulfide Coated with Reduced Graphene Oxide and Carbon for High-Capacitance Supercapacitor. Journal of Nanoscience and Nanotechnology, 2017, 17, 4091-4098.	0.9	5
263	Effects of doping La and Cu on photoinduced charge properties of TiO2 and its relationships with photocatalytic activity. Science in China Series B: Chemistry, 2006, 49, 345-350.	0.8	3
264	Theoretical study on the reaction mechanism of CN radical with ketene. Science in China Series B: Chemistry, 2008, 51, 101-110.	0.8	3
265	Innenrücktitelbild: Ultrathin Porous Carbon Nitride Bundles with an Adjustable Energy Band Structure toward Simultaneous Solar Photocatalytic Water Splitting and Selective Phenylcarbinol Oxidation (Angew. Chem. 9/2021). Angewandte Chemie, 2021, 133, 5003-5003.	2.0	1